Computerized methods for determining respiratory phase on dynamic chest radiographs obtained by a dynamic flat-panel detector (FPD) system

著者	Tanaka Rie, Sanada Shigeru, Kobayashi Takeshi, Suzuki Masayuki, Matsui Takeshi, Matsui Osamu
journal or publication title	Journal of Digital Imaging
volume	19
number	1
page range	41-51
year	2005-03-01
URL	http://hdl.handle.net/2297/1658

Title of article

Computerized methods for determining respiratory phase on dynamic chest radiographs obtained by a dynamic flat-panel detector (FPD) system

Authors

Rie Tanaka[1], Shigeru Sanada[1], Takeshi Kobayashi[2], Masayuki Suzuki[1], Takeshi Matsui[2], Osamu Matsui[2]

Affiliations

[1] School of Health Sciences, Faculty of Medicine, Kanazawa University

[2] Department of Radiology, Kanazawa University Hospital

Corresponding Author

Rie Tanaka

E-mail: rie44@mhs.mp.kanazawa-u.ac.jp

TEL: 81-76-265-2537

FAX: 81-76-234-4366

Mailing address: School of Health Sciences, Faculty of Medicine, Kanazawa University; 5-11-80 Kodatsuno, Kanazawa, 920-0942, Japan

This work was partially supported by Canon Inc., Tateishi Science and Technology Foundation, and a Grant-in-Aid from the Japanese Ministry of Education, Culture, Sports, Science and Technology.

Abstract

Chest radiography using a dynamic flat-panel detector with a large field of view can provide sequential chest radiographs during respiration. These images provide information regarding respiratory kinetics, which is effective for diagnosis of pulmonary diseases. For valid analysis of respiratory kinetics in diagnosis of pulmonary diseases, it is crucial to determine the association between the kinetics and respiratory phase. We developed four methods to determine the respiratory phase based on image information associated with respiration, and compared the results in dynamic chest radiographs of 37 subjects. Here, the properties of each method and future tasks are discussed. The method based on the change in size of the lung gave the most stable results, and that based on the change in distance from the lung apex to the diaphragm was the most promising method for determining the respiratory phase.

Keyword: respiratory phase, plat-panel detector (FPD), computer analysis, diaphragm, diagnosis

Introduction

Chest radiography using a recently developed dynamic flat-panel detector (FPD) with a large field of view can provide sequential chest radiographs during respiration. These images provide not only anatomical information but also respiratory kinetics, such as the diaphragmatic movement and respiratory changes in X-ray translucency in the local lung area.

Many investigators have attempted to obtain such respiratory kinetics using image-based examinations, such as X-ray fluoroscopy,[1,2] dynamic magnetic resonance imaging (MRI),[3-5] and pulmonary computed tomography (CT).[6,7] This kinetic information is effective for diagnosing chronic obstructive pulmonary disease (COPD) and restrictive pulmonary disease,[6] for making decisions pertaining to lung volume reduction surgery (LVRS), and for observing postoperative progress.[3-5] However, these methods are not practiced as routine examinations due to various limitations, such as the small field of view, temporal resolution, and high dose of exposure.

Therefore, we investigated methods for quantifying respiratory kinetics on dynamic chest radiographs obtained easily using an FPD system.[8,9] The results showed that imaging using dynamic FPD could capture the respiratory changes, such as diaphragmatic movement and respiratory changes in X-ray translucency in local lung area associated with ventilation. To establish this new system for diagnosis of pulmonary diseases based on respiratory kinetics, it was crucial to determine the association between the kinetics and respiratory phase.

There is a need to increase the accuracy of radiation therapy of lung tumors, which move during respiration. This has been achieved by measuring the moving area of the lung tumor by fluoroscopy and setting an appropriate margin based on the moving area

in radiation therapy planning.[10] Real-time tumor tracking in radiation therapy using fluoroscopy has also been used.[11,12] In this method, gold markers embedded near the target are traced under fluoroscopic guidance. We feel that computerized methods for determination of respiratory phase based on image information are also needed for radiation therapy. For example, computerized methods will assist in the planning of radiation therapy and in improving both its efficiency and accuracy, and will also improve the accuracy of tumor tracking by providing real-time direction from respiratory phase based on image information.

As described above, the determination of respiratory kinetics represents important clinical information. However, the kinetics of respiration can only be evaluated subjectively by visual observation. Previously, we developed a method for determining respiratory phase based on diaphragmatic movement.[9] However, there were still some issues to be resolved before this method could be used for determining respiratory phase. Respiration is a passive movement caused by the diaphragm and intercostal muscles, and many types of lung structure, *i.e.*, the rib cage, pulmonary vessels, and bronchi, are also moved during breathing.[13,14] Therefore, we attempted to determine respiratory phase based on many kinds of image information associated with respiration on sequential chest radiographs.

The present study was performed to develop and investigate the accuracy of several methods for determining respiratory phase on sequential chest radiographs obtained using a dynamic FPD system.

Materials and Methods

Image acquisition

Posteroanterior (PA) dynamic chest radiographs during respiration were obtained with 30 frames in 10 seconds using a modified FPD system (CXDI-40G, Canon Inc., Tokyo, Japan), X-ray device (KXO 80G, Toshiba, Tokyo, Japan), and X-ray tube (DRX 2724HD 0.6/1.2, Toshiba) (Fig. 1). The modified FPD was an indirect type made of GOS (Gd^2O^2S (Tb)), and was capable of taking images at up to 6 frames per second. Exposure conditions were 110 kV, 80 mA, 6.3 ms, 2.0 mm Al filter, 3 frames per second, and SID = 2 m. The matrix size was 1344×1344 pixels, the pixel size was 320×320 μm, and the gray-level range of the images was 4096. Low pixel values were related to dark areas in the images and these in turn were related to high X-ray translucency in this system. The investigation was performed in 37 subjects, including 29 healthy controls and 8 subjects with pulmonary diseases (Table 1). The subjects were instructed to respire according to an automated voice (Fig. 2), and the manner of breathing was practiced before imaging. The total entrance surface dose, measured in air without backscattering, was approximately 0.4 mGy, which was 1.5-fold greater than that of conventional PA chest radiography using a Fuji Computed Radiography system (Fuji Medical Systems Co., Ltd., Tokyo, Japan) in our hospital. Approval for this study was obtained from our institutional review board, and each of the patients gave their written informed consent to participation.

Image analysis

The analysis was performed on a personal computer (Operating system, Windows 2000, Microsoft, Redmond, WA, USA; CPU, Pentium 4, 2.6 GHz; Memory, 1 GB) with our algorithm described below (Development environment: C++Builder; Borland, Scotts Valley, CA, USA). The movement of the diaphragm and chest wall directly reflects the

respiratory phase, because respiration is a passive movement caused by the diaphragm and intercostal muscles.[13] Therefore, we developed methods to quantify the following four measures associated with respiration and then determined respiratory phase based on the results.

1. Distance from the lung apex to the diaphragm
2. Summation of pixel values in the region of interest (ROI) covering both lung fields

   Size of lung fields
3. Correlation coefficient between each frame and a minimum intensity projection (MINIP) image created from dynamic chest radiographs
4. Summation of respiratory vectors in the area near the diaphragm

Method 1: Measurement of the distance between the lung apex and diaphragm

Respiration is a passive action caused by the diaphragm and intercostals muscles. Thus, descent of the diaphragm indicates inspiration and ascent of the diaphragm indicates expiration. This method based on the distance from the lung apex to the diaphragm level measured by the edge detection technique consisted of two steps, *i.e.*, determination of the points for measurement on the first frame and subsequent tracing of the points (Fig. 3). This method might be sensitive because it involves direct measurement of the diaphragm. The rib cage and mediastinum edge locations in the first frame were determined from the first derivatives of the horizontal signature in the middle of the image (Fig. 4a). The diaphragm edge locations were then determined from the first derivatives of the vertical signature on the midpoint between locations of the peripheral rib cage edge and the mediastinum edge (Fig. 4b). The lung apex edge locations were determined continuously from the first derivatives of the vertical

signature on the midpoint between locations of the mediastinum edge and the diaphragm edge (Fig. 4c). In determination of the lung apex edge locations, the three largest edges were selected as candidates and then the uppermost edge was determined as the lung apex edge to prevent incorrect determination of clavicle edges. Figure 4d shows the points used to determine the distance from the lung apex to the diaphragm. After the second frame, dynamic chest radiographs were processed with a 7×7 Sobel filter to enhance the edges of the diaphragm (Fig. 5a). The points for measurement decided in the first frame were traced after the second frame with the sequential similarity detection algorithm (SSDA)[15], where the ROIs including the points for measurement in the previous frame were used as a template (Fig. 5b) (eq. 1). The sizes of the ROIs were 50×50 for the lung apex and 50×100 for the diaphragm, and those of the search areas were 70×70 for the lung apex and 58×180 for the diaphragm, because the movement of lung structures along the cephalocaudal axis is more extensive than that along the horizontal axis. The difference (D) between the search area in the next frame, $f_{n+1}(x_i+dx, y_j+dy)$, and the ROI in the current frame, $f_n(x_i, y_j)$, was expressed as follows:

$$D = \sum_j \sum_i \left| f_{n+1}(x_{ni} + dx, y_{nj} + dy) - f_n(x_{ni}, y_{nj}) \right| \qquad (1)$$

$$Lung\ \ apex: 0 \le i < 50, \quad 0 \le j < 50, \quad -10 \le dx < 10, \quad -10 \le dy < 10, \quad 1 < n < 29$$

$$Diaphragm: 0 \le i < 50, \quad 0 \le j < 100, \quad -4 \le dx < 4, \quad -40 \le dy < 40, \quad 1 < n < 29$$

The smallest D resulted from the matching ROI of the current frame on the most similar search area in the next frame. The distance of the measured points from frame # n to frame # n+1 was determined as *dx* and *dy* by minimizing D and the coordinates of the points after movement were expressed as (x_{ni} + *dx*, y_{nj} + *dy*). The template was also

renewed with every frame, as $x_{(n+1)i} = (x_{ni} + dx)$ and $y_{(n+1)j} = (y_{nj} + dy)$, so that accurate tracking could be achieved readily.

Method 2: Summation of pixel values in ROI covering both lung fields

This method was based on summation of pixel values in the region of interest (ROI) covering both lung fields, which were proportional to the sizes of the lung fields (Fig. 6). The lung volume increased in inspiration and decreased in expiration, these changes were expressed as the changes in the sizes of the lung fields. This method was simple throughout the whole process except for location of a large ROI. Thus, relatively stable results were expected. In the first frame, the rib cage edge locations were determined from the first derivatives of the horizontal signature in the middle of the image, and then a large ROI was located on the lung fields as shown in Fig. 7. The sum of the pixel values in the ROI was calculated throughout 30 frames. The respiratory phase was determined based on the first derivatives of the summation of the pixel value curve (Fig. 8).

Method 3: Correlation coefficient between each frame and the minimum intensity projection (MINIP) image

This method was based on the correlation coefficient (r) between each frame $F_n(i, j)$ and a template image $M_n(i, j)$ created from dynamic chest radiographs (Fig. 9):

$$r = \frac{\sum_j \sum_i \left\{F_n(i,j) - \overline{F_n(i,j)}\right\}\left\{M(i,j) - \overline{M(i,j)}\right\}}{\sqrt{\sum_j \sum_i \left\{F_n(i,j) - \overline{F_n(i,j)}\right\}^2 \sum_j \sum_i \left\{M(i,j) - \overline{M(i,j)}\right\}^2}} \qquad (2)$$

$0 < i < 1344, \quad 0 < j < 1344, \quad 1 < n < 30$

The MINIP image represented the maximum inspiratory phase, and the maximum

intensity projection (MIP) image represented the maximum expiratory phase (Fig. 10). Thus, respiratory condition was estimated as the maximum inspiration when the correlation coefficient using the MINIP image as a template was at the maximum value, and respiratory condition was estimated as the maximum expiration when the correlation coefficient using the MIP image as a template was at the maximum value (Fig. 11). This method is advantageous in terms of simple process freeing of edge detection, which is accompanied by a larger risk of detection error.

Method 4: Summation of respiratory vectors in the area near the diaphragm

This method was based on summation of the respiratory vectors of lung structures near the diaphragm (Fig. 12). Lung vessels and bronchi near the diaphragm show a large degree of movement in the cephalocaudal direction during respiration. This method had the ability to catch even small respiratory motion of lung vessels and bronchi as compared to other methods, because smaller local areas were used for detecting respiratory vectors. These respiratory vectors were represented as their summation, and used to determine respiratory phase.

First, the respiratory vectors (dx, dy) were measured by the block matching technique. The local area (50×50 pixels) in the frame being examined was searched for the most similar local area in the range of 82×110 pixels in the previous frame as described elsewhere in detail.[9] The difference (D) between the previous local area, $f_{n-1}(x_i + dx, y_j + dy)$, and that being examined, $f_n(x_i, y_j)$, was expressed as follows:

$$D = \sum_j \sum_i \left| f_n(x_i, y_j) - f_{n-1}(x_i + dx, y_j + dy) \right| \qquad (3)$$

$$-16 \le dx < 16, \quad -30 \le dy < 30, \quad 1 \le n < 30,$$

$$0 \le i < 50, \quad 0 \le j < 50$$

The smallest *D* value resulted when there were more similarities in the previous local area and that being examined. The respiratory vectors (*dx*, *dy*) in the local area were determined by minimizing *D*. The respiratory vectors calculated by equation (3) show the directions of movement and distance of the local area from the previous frame to that being examined. Second, the diaphragm edge locations were determined by the same procedure as described in "Method 1," and then the summed respiratory momentum in the cephalocaudal direction (*dy*) was calculated in the ROIs centered on the diaphragm edge locations as shown in Fig. 13. One side of the ROI was 250 pixels, which was about the same size as the width of the lung field. Figure 14 shows the summation of *dy* throughout all frames. Negative and positive values were taken to indicate respiratory phase and inspiratory phase, respectively.

Manual measurement

Three experts determined the respiratory phase based on the movement of the diaphragm, rib cage, lung vessels, and ribs by observing the images in each frame (Table 2). When there were differences between their determined frame number of transition from expiratory phase to inspiratory phase or *vice versa*, the averaged frame number was adopted.

Evaluation of the results

We evaluated the results obtained by the four methods by comparison to the results of manual measurements. We used the transition of respiratory phase as reference frames to assess errors. "Non-error" was defined when there were no differences between reference frames decided by manual measurement and those determined by

computerized methods. We also defined “One error” when there was only a difference in one frame between them, and “Within three frames” when there was a difference within 3 frames between them. “Within three frames” was based on the observation that there were slight differences in three frames around breath-holding.

Results

The results obtained by our four methods are shown in Table 3. Method 1 was capable of determining the points for measurement almost exactly except for the left diaphragm, and the points could be traced with a high degree of accuracy (Table 4). However, the overall results obtained by these two procedures, *i.e.*, determination and subsequent tracing of the points for measurement, did not achieve a high score. The points for measurement that were corrected manually were traced, and this method was shown to be able to determine the respiratory phase accurately in 36 of 37 cases (97.3%) within 3 frames of error as shown in Table 3. On the other hand, method 2 was capable of determining the respiratory phase with an accuracy of 91.9% within 3 frames of error. In contrast to our expectations, the accuracy of method 3 was poor; respiratory phase could be determined with an accuracy of only 45.9% within 3 frames of error. Although the maximum inspiratory phase was determined accurately, the maximum expiratory phase was determined with 3~7 frames of error. Method 4 was able to determine the respiratory phase accurately in 28 of 37 cases (75.7%) within 3 frames of error.

Discussion and conclusion

Method 1 could determine not only respiratory phase but also respiratory level because the diaphragm level was measured directly. However, it is still necessary to

improve the accuracy in determining the lung apex and diaphragm points used for measurement. In particular, for the left diaphragm, many errors occurred due to incorrect detection of gas in the stomach, the edge of the heart, and edges of the breast in female subjects instead of the diaphragm edge. Some other measures are needed for correction of these errors. Furthermore, in the subject with pneumonia, the interstitial pattern made it difficult to recognize the diaphragm edge locations. The results suggested that it was possible that the performance of this method would be decreased in cases with an interstitial pattern. However, the points traced during respiration achieved a high degree of accuracy. Thus, if the accuracy of determination of the points for measurement could be improved, method 1 would be promising for determination of the respiratory phase.

In method 2, there was no need to determine edge locations as this method had less error than that involving direct measurement of diaphragm movement. However, this method could not detect subtle differences in respiratory level, such as the end of expiration or inspiration. In such phases, there was little movement of the diaphragm and rib cage, and so the results were affected by the heartbeat. Measurement by a ROI hollowed-out the mediastinum area may be effective to overcome this problem. This method is expected to be effective for subjects in whom the diaphragm is visually imperceptible. Thus, method 2 might be suitable for rough estimation of respiratory phase.

In contrast to our expectations, method 3 did not show satisfactory accuracy. The MINIP image was unsuitable as a template. The MINIP image represented the image in the maximum expiratory phase, but there were some differences in imaging gas of the stomach and the waist in the MINIP image in comparison with the maximum expiratory

image. These differences resulted in the concave part of the correlation coefficient curve indicated by the arrow in Fig. 12, which should actually be convex because this is in the maximum expiratory phase. As shown in Fig. 12, a concave curve in this part was often observed in many subjects. This method would thus be suitable only for ROI locations not including the abdomen area.

The accuracy of method 4 was affected markedly by movement of the heart and ribs. In addition, many errors were caused by physical motion in some frames. It is necessary to develop a method for differentiating between respiratory movement and movement caused by the heartbeat. It is also necessary to investigate the location and size of the ROIs.

In this study, we developed several methods primarily to determine respiratory phase on sequential chest radiographs during respiration for diagnosis of pulmonary diseases. From the results, we concluded that the method based on summation of pixel value in the ROI (Method 2) was most stable, and that based on distance from the lung apex to the diaphragm (Method 1) was the most promising method for determining respiratory phase. Information about respiratory phase obtained from the above methods would improve the accuracy of image analysis, such as sequential lung recognition and the tracing of certain targets in the lung. We are also considering applying these techniques in a clinical setting, such as in radiation therapy tracing a target in the lung under respiration.

Further studies are required to improve the accuracy of determination of respiratory phase by developing a complex method with method 2 as pre-processing and method 1 as the main processing. For example, method 2 could be used for rough estimation of respiratory phase. Images emphasizing the moving area of the diaphragm can then be

produced by subtraction from those in the maximum inspiratory phase and in the maximum expiratory phase. This moving area of the diaphragm will be useful for judging errors in determination of the diaphragm edge locations in method 1.

References

1. Lam KL, Chan HP, MacMahon H, et al: Dynamic digital subtraction evaluation of regional pulmonary ventilation with nonradioactive xenon. Invest Radiolo. 25: 728-735, 1990
2. Singh B, Panizza JA, and Finucane E: Breath-by-breath measurement of the volume displaced by diaphragm motion. J Appl Physiol. 94:1084-1091, 2003
3. Suga K, Tsukuda T, Awaya H, el al: Impaired respiratory mechanics in pulmonary emphysema. evaluation with dynamic Breathing MRI. JMRI 10:510-520, 1999
4. Unal O, Arslan H, Uzun K, et al: Evaluation of diaphragmatic movement with MR fluoroscopy in chronic obstructive pulmonary disease. Clin Imaging. 24:347-350, 2000
5. Etlick O, Sakarya ME, Uzun K, et al: Demonstrating the effect of theophylline treatment on diaphragmatic movement in chronic obstructive pulmonary disease patients by MR-fluoroscopy. Eur J Radiol. 51:150-154, 2004
6. David M, Athol U, Michael B, el al: Bronchiectasis: Functional significance of areas of decreased attenuation at expiratory CT. Radiology 193:369-374, 1994
7. Shirakawa T, Fukuda K, Miyamoto Y, et al: Parietal pleural invasion of lung masses: evaluation with CT performed during deep inspiration and expiration. Radiology. 192:809-811,1994
8. Tanaka R, Sanada S, Suzuki M, et al: Automated analysis for the respiratory kinetics with the screening dynamic chest radiography using a flat-panel detector system. Pro - CARS 2003, 179-186, 2003
9. Tanaka R, Sanada S, Kobayashi T, et al: Breathing Chest Radiography using a Dynamic Flat-Panel Detector (FPD) Combined with Computer Analysis. Med Phys. 31:2254-2262, 2004
10. Ruschin M and Sixel KE: Integration of digital fluoroscopy with CT-based radiation therapy planning of lung tumors. Med Phys. 29: 1698-1709, 2002.
11. Seppenwoolde Y, Shirato H, Kitamura K, et al: Precise and real-time measurement of 3D tumor motion in lung due to breathing and heartbeat, measured during radiotherapy. Int J Radiat Oncol Biol Phys. 53:822-834, 2002

12. Shirato H, Harada T, Harabayashi T, et al: Feasibility of insertion/implantation of 2.0-mm-diameter gold internal fiducial markers for precise setup and real-time tumor tracking in radiotherapy. Int J Radiat Oncol Biol Phys. 56:240-247, 2003
13. West JB (1995) Mechanics of breathing. In: *Respiratory Physiology* – the essentials 5th ed. Williams & Wilkins, Baltimore, Philadelphia, Hong Kong, London, Munich, Sydney, Tokyo, 89-116.
14. Squire LF and Novelline RA (1998) Overexpansion and Collapse of the Lung. In: Fundamentals of Radiology, 4th ed., Harvard University Press, Cambridge, Massachusetts, and London, England, pp 88-89
15. Barnea DI, Silverman HF: A Class of Algorithms for Fast Digital Image Registration. IEEE Trans. Comput. c-21, 179-186, 1972.

Legends for illustrations

Fig. 1 Dynamic chest radiographs in a healthy subject

Fig. 2 Imaging method.

Fig. 3 Flowchart of method 1.

Fig. 4 (a) Determination of the edge locations for the ribs and mediastinum. Determination of the points for measurement in (a) the lung apex and (b) the diaphragm. (c) The points for measurement.

Fig. 5 (a) Dynamic chest radiographs with edges enhanced by Sobel-filter. (b) Tracing the points for measurement.

Fig. 6 Flowchart of method 2.

Fig. 7 Location of a large ROI.

Fig. 8 Summation of pixel value curves.

Fig. 9 Flowchart of method 3.

Fig. 10 (a) MIP image and (b) MINIP image created from 30 frames of dynamic chest radiographs. (c) Image in the maximum expiratory phase. (d) Image in the maximum inspiratory phase.

Fig. 11 Correlation coefficient curve

Fig. 12 Flowchart of method 4.

Fig. 13 Locations of two ROIs centered on the diaphragm edge locations.

Fig. 14 Summation of the respiratory vectors curve.

Table 1 Subjects in the present study.

Table 2 Standards for deciding respiratory phase

Table 3 Total results.

Table 4 Separate accuracy of determination of the points for measurement and tracing

of the points in method 1.

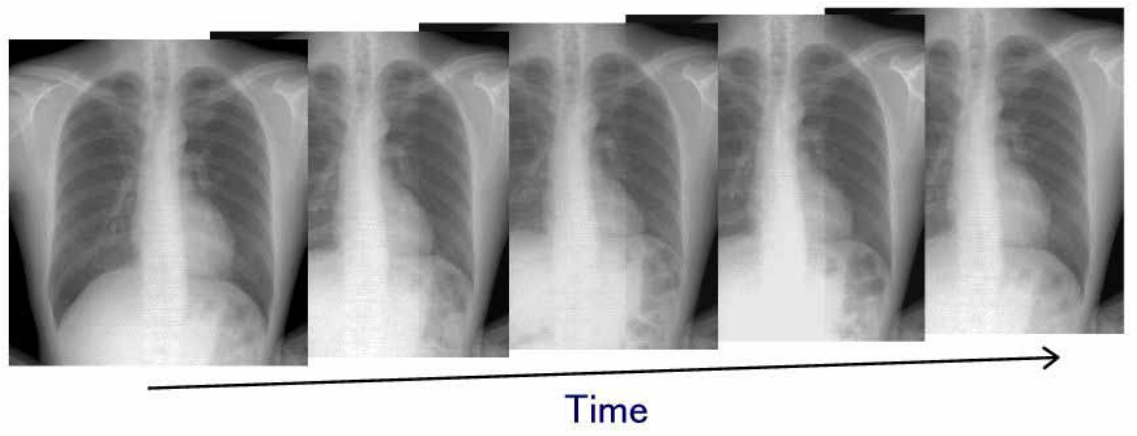
Time

Fig. 1

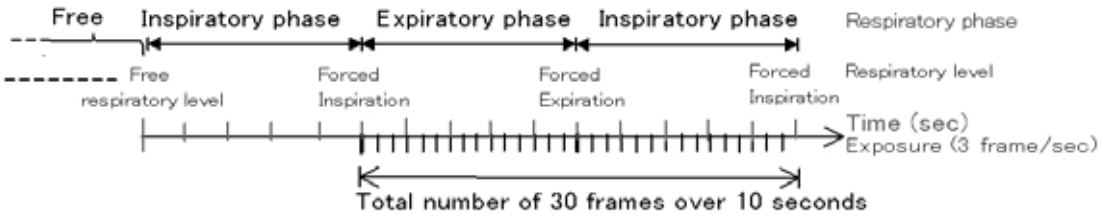
Free
Inspiratory phase
Expiratory phase
Inspiratory phase
Respiratory phase
Free respiratory level
Forced Inspiration
Forced Expiration
Forced Inspiration
Respiratory level
Time (sec)
Exposure (3 frame/sec)
Total number of 30 frames over 10 seconds

Fig. 2

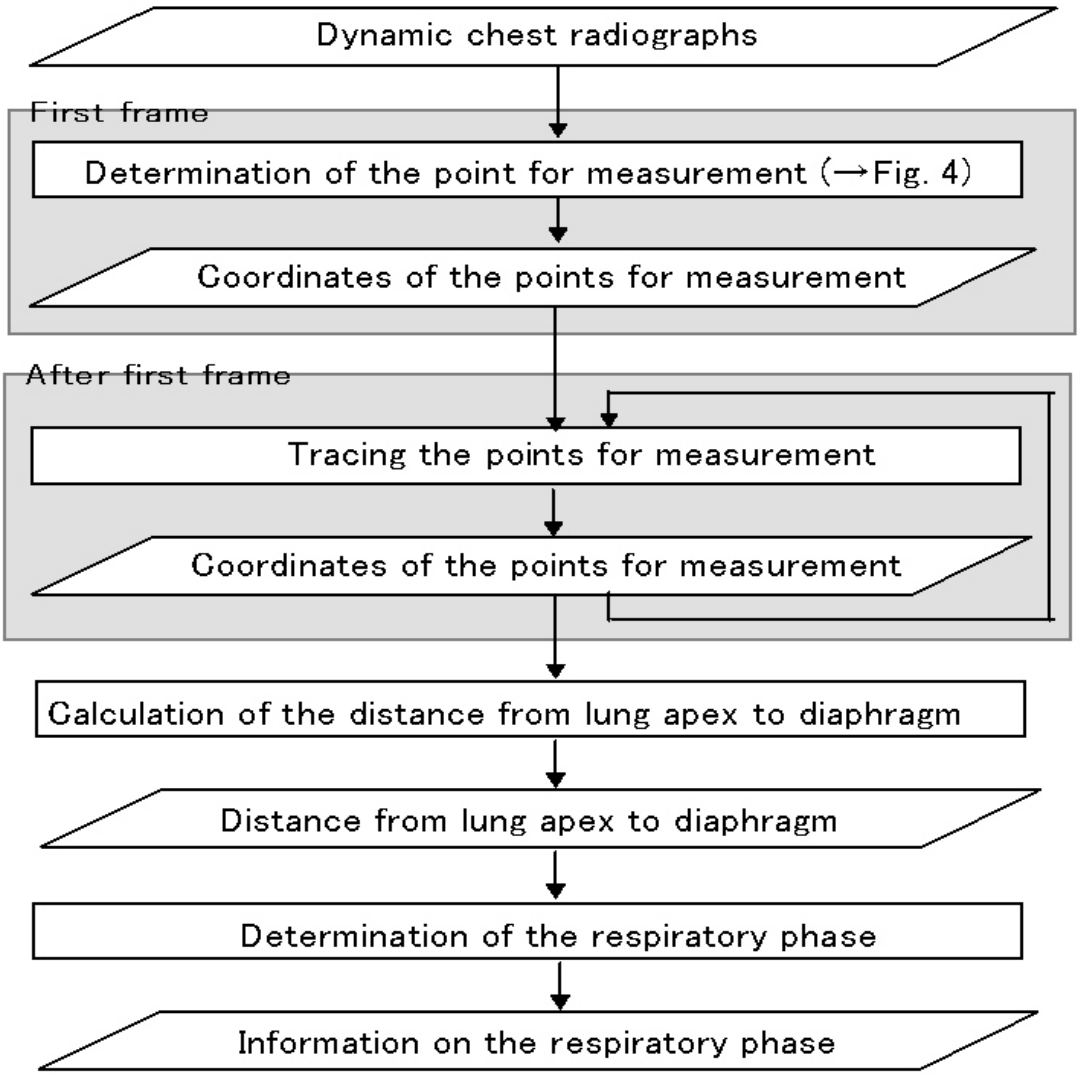
Dynamic chest radiographs
First frame
Determination of the point for measurement (→Fig. 4)
Coordinates of the points for measurement
After first frame
Tracing the points for measurement
Coordinates of the points for measurement
Calculation of the distance from lung apex to diaphragm
Distance from lung apex to diaphragm
Determination of the respiratory phase
Information on the respiratory phase

Fig. 3

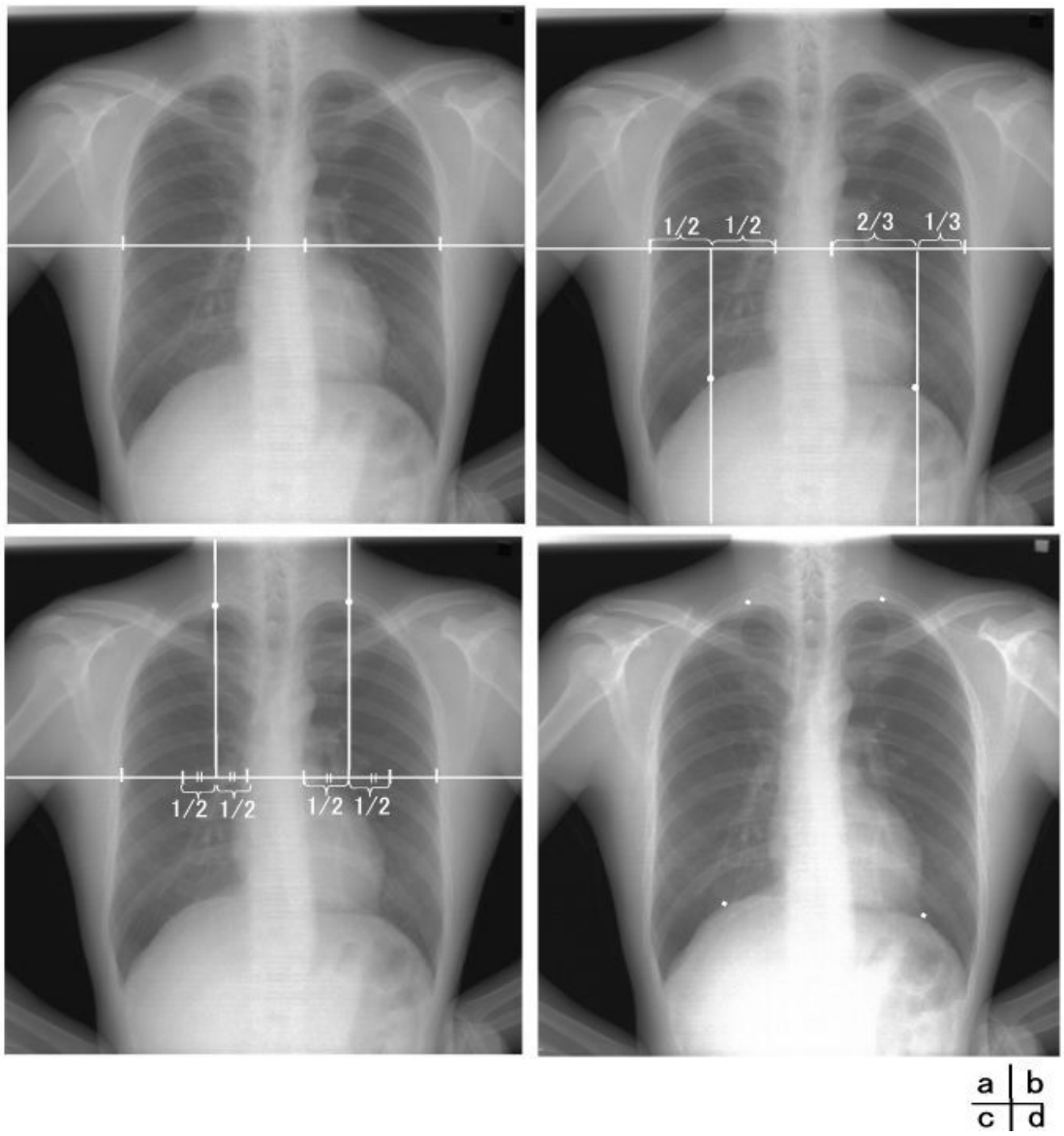

Fig. 4

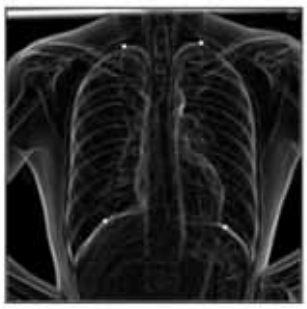

Fig. 5a

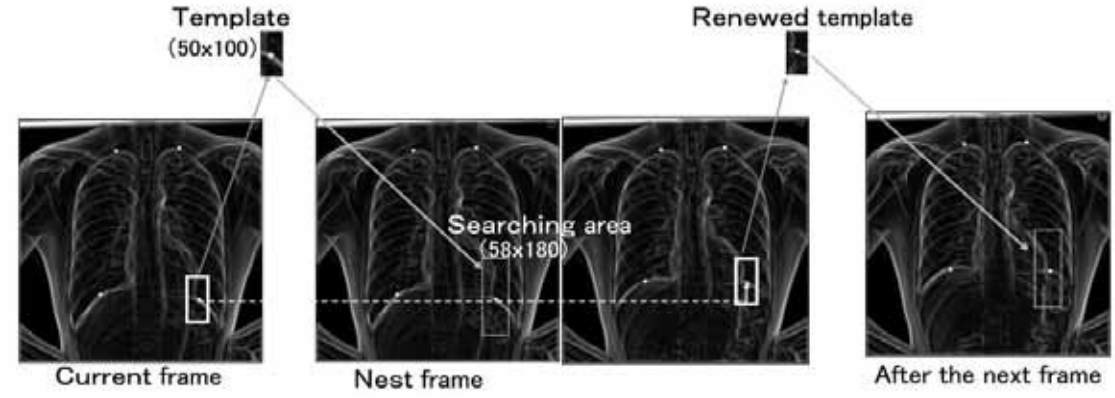

Fig. 5b

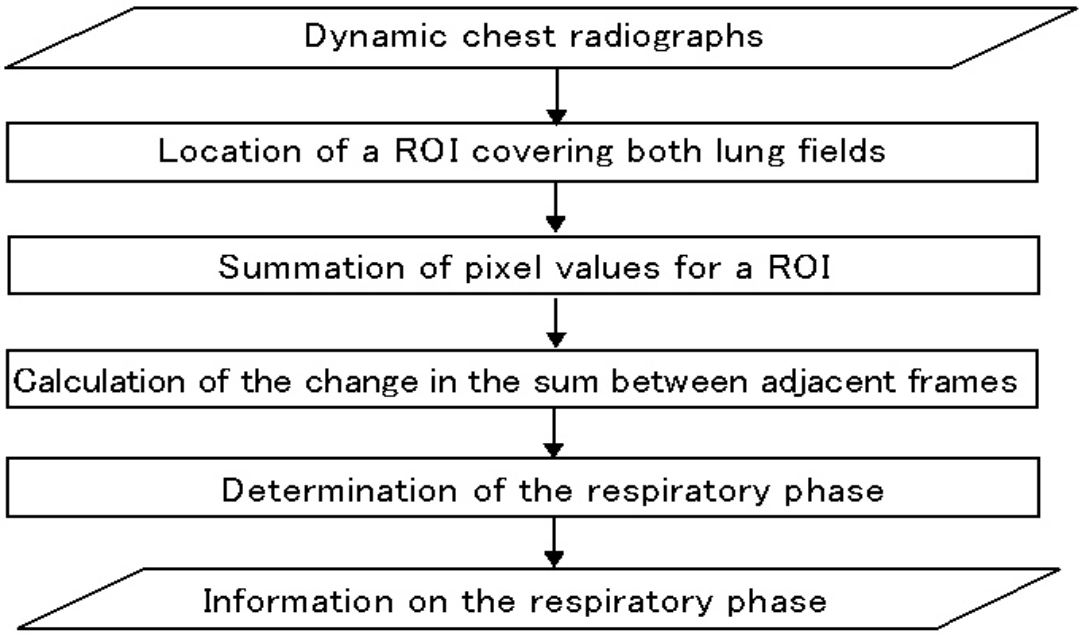

Fig .6

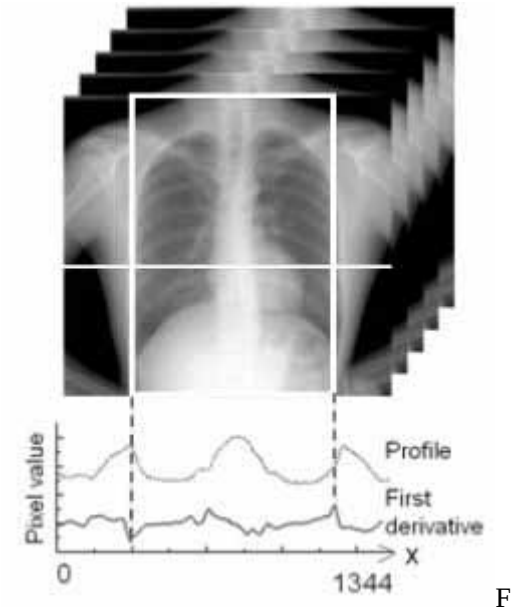
Pixel value
Profile
First
derivative
X
0
1344

Fig. 7

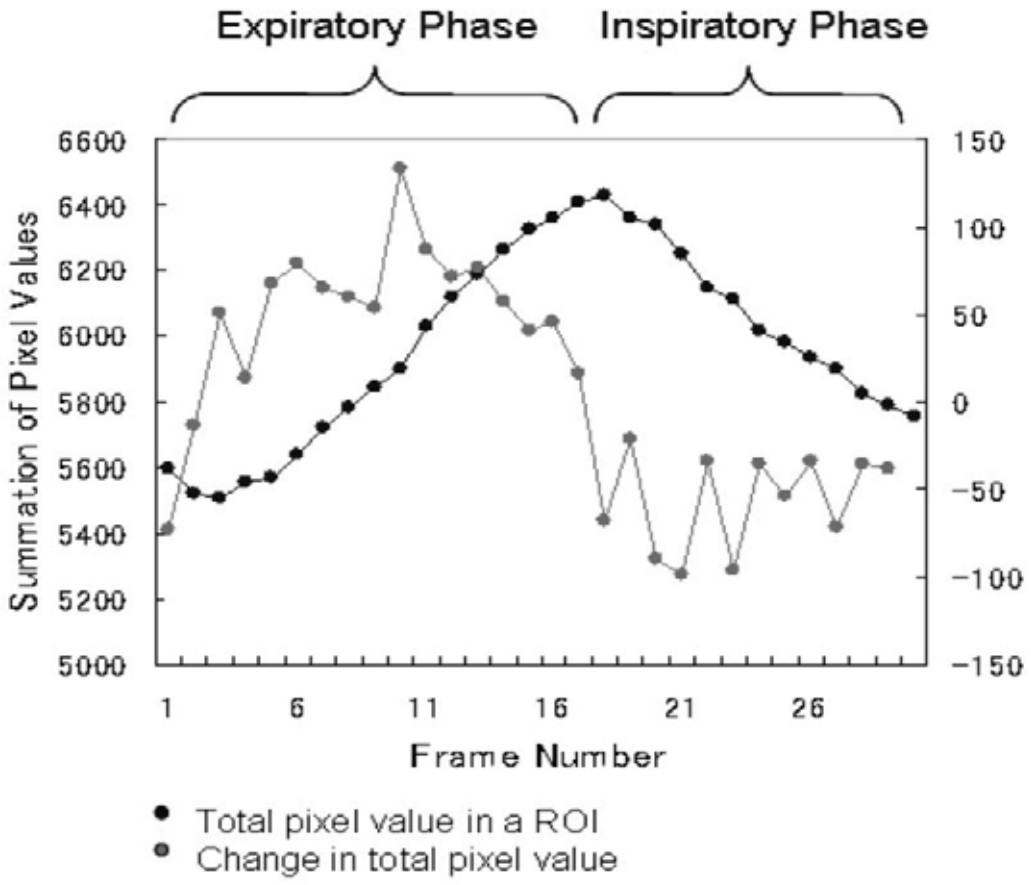
Expiratory Phase
Inspiratory Phase
Summation of Pixel Values
6600
6400
6200
6000
5800
5600
5400
5200
5000
150
100
50
0
−50
−100
−150
1
6
11
16
21
26
Frame Number
Total pixel value in a ROI
Change in total pixel value

Fig. 8

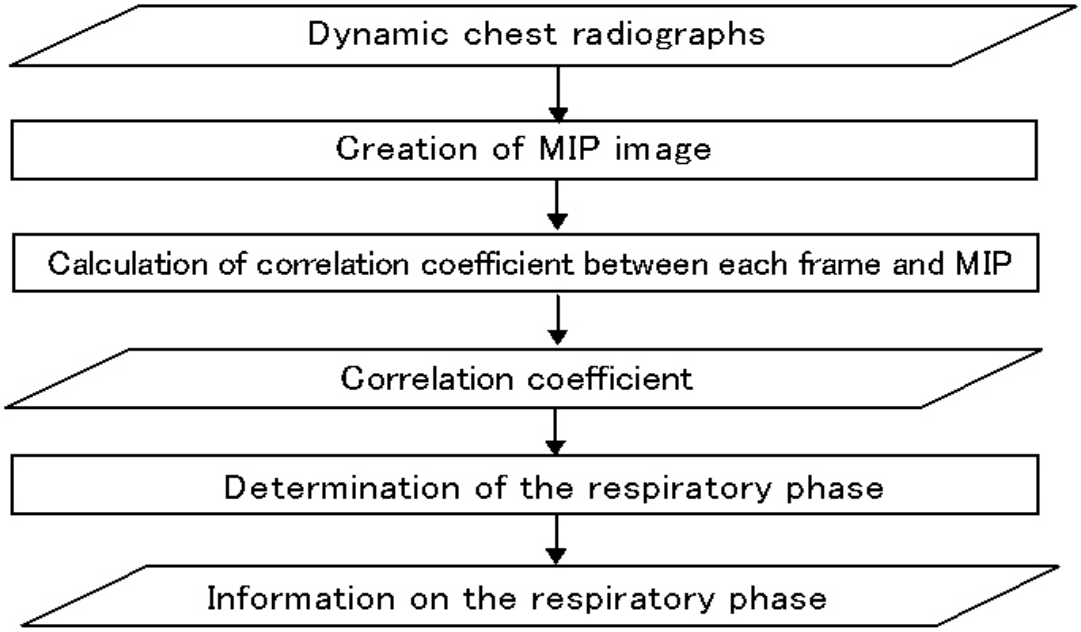
Dynamic chest radiographs
Creation of MIP image
Calculation of correlation coefficient between each frame and MIP
Correlation coefficient
Determination of the respiratory phase
Information on the respiratory phase

Fig. 9

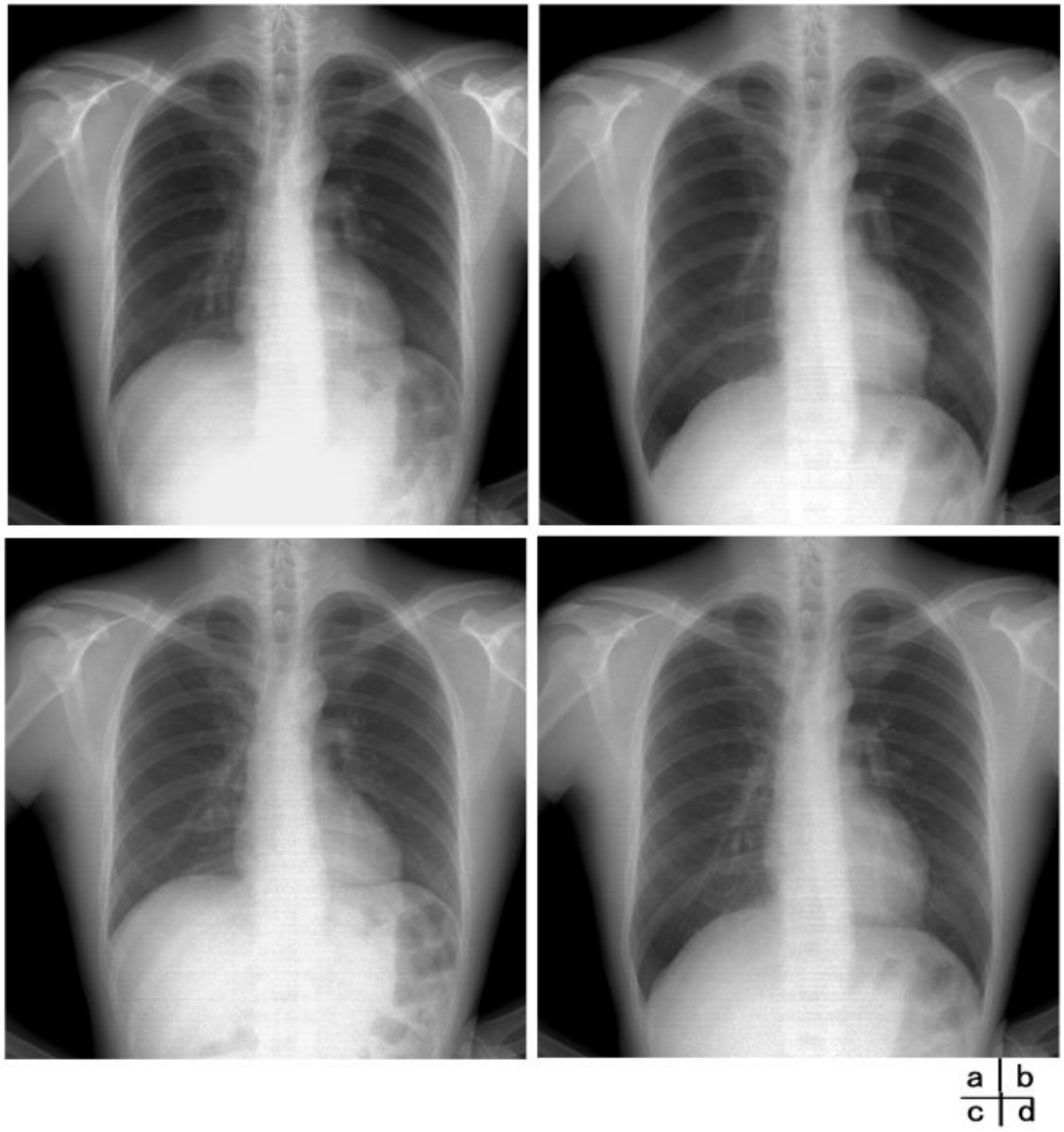

Fig. 10

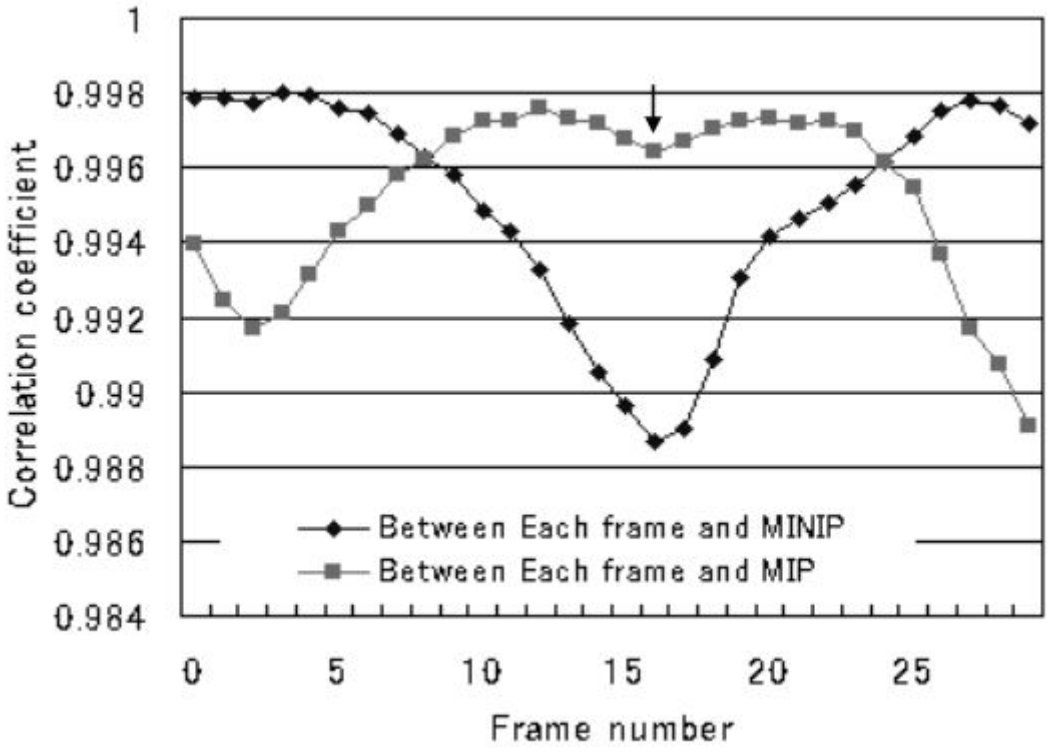
1
0.998
0.996
0.994
0.992
0.99
0.988
0.986
0.984
Correlation coefficient
Between Each frame and MINIP
Between Each frame and MIP
0
5
10
15
20
25
Frame number

Fig. 11

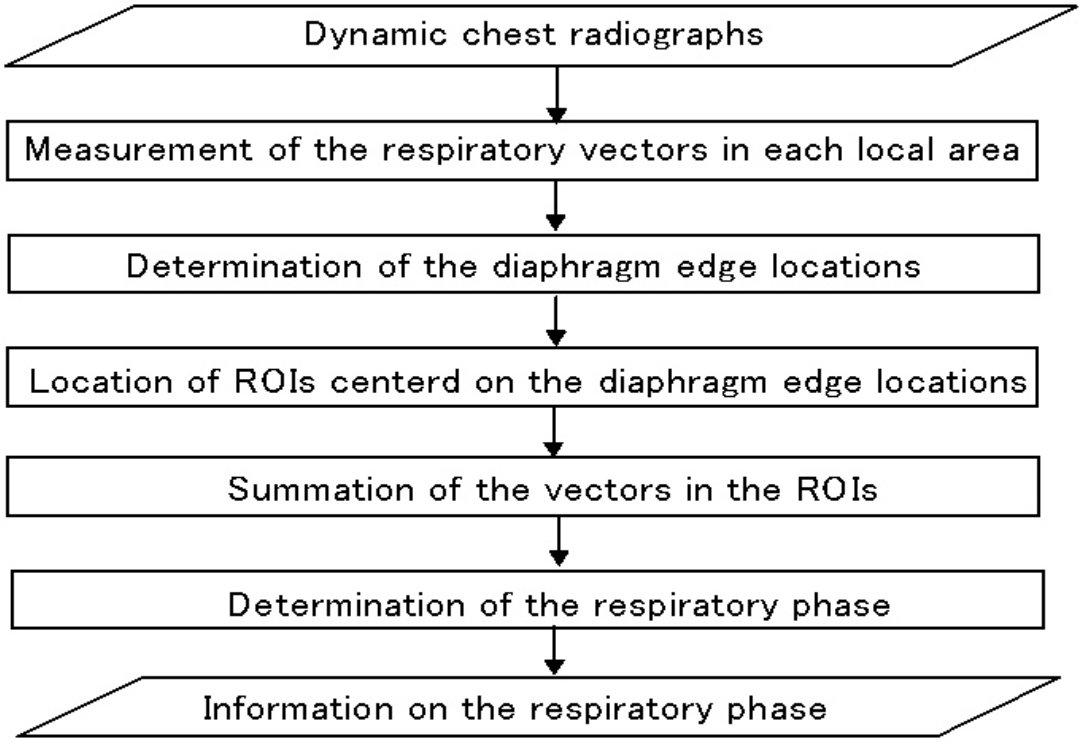
Dynamic chest radiographs
Measurement of the respiratory vectors in each local area
Determination of the diaphragm edge locations
Location of ROIs centerd on the diaphragm edge locations
Summation of the vectors in the ROIs
Determination of the respiratory phase
Information on the respiratory phase

Fig. 12

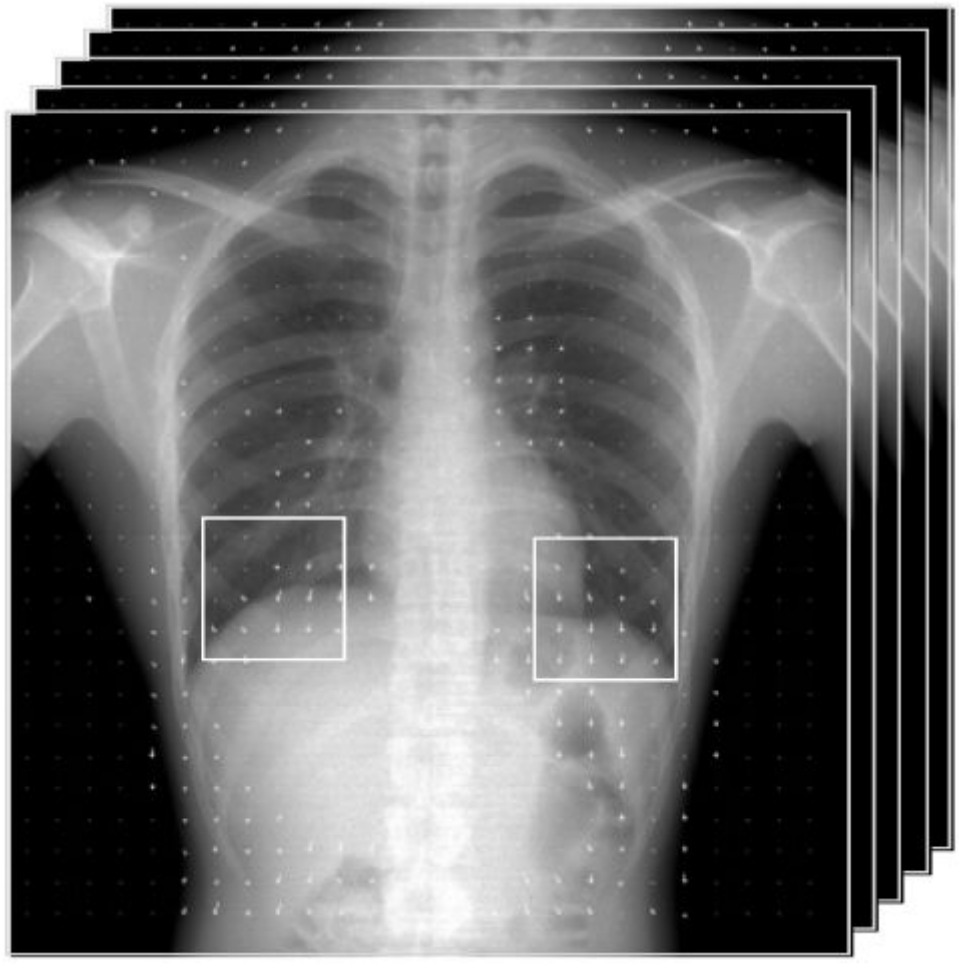

Fig. 13

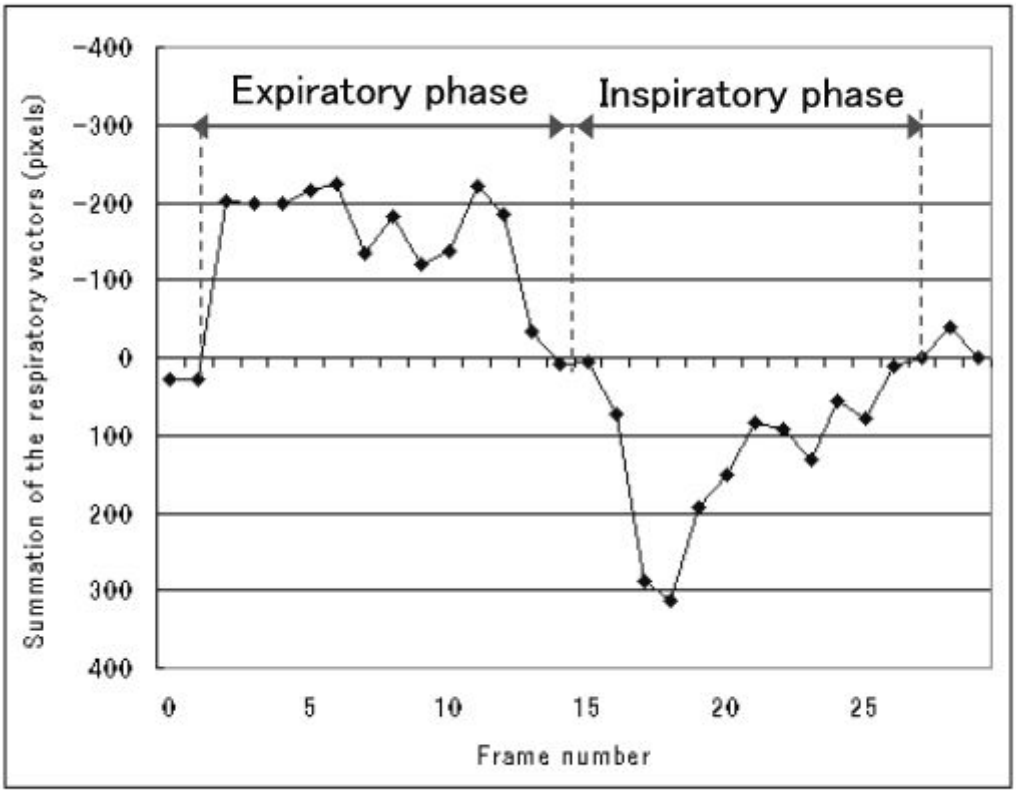
Expiratory phase
Inspiratory phase
Summation of the respiratory vectors (pixels)
-400
-300
-200
-100
0
100
200
300
400
0
5
10
15
20
25
Frame number

Fig. 14

Subjects	Number
Healthy subjects	29 (21~55 years old, Mean: 31.0, M:F=25:4)
Subjects with pulmonary diseases	8 (31~75 years old, Mean: 57.6, M:F=5:3)
Pneumonia	4
Emphysema	2
Bronchial asthma	1
Nodular pulmonary disease	1

Table1

	Moving direction of diaphragm	Moving direction of rib cage	Moving direction of Lung vessels
Inspiratory phase	Downside	Outside	Downside
Exspiratory phase	Upside	Inward	Upside
Breath-holding	Non	Non	Non

Table 2

	Complete	With one frame error	Within three frames error
Method 1	75.7 (28/37)	91.9 (34/37)	97.3 (36/37)
Method 2	43.2 (16/37)	70.3 (26/37)	91.9 (34/37)
Method 3	2.7 (1/37)	18.9 (7/37)	45.9 (17/37)
Method 4	59.5 (22/37)	67.6 (25/37)	75.7 (28/37)

Table 3 Unit (%)

	Lung apex		Diaphragm	
	Right	Left	Right	Left
Determination of the points	81.6	76.7	84.2	42.1
Tracing the points	100	100	97.4	78.9
As a whole	81.6	76.7	82.0	33.2

Table 4 Unit (%)